CrystEngComm

Accepted Manuscript

ROYAL SOCIETY OF CHEMISTRY

www.rsc.org/crystengcomm

CrystEngComm RSCPublishing

ARTICLE

Two-dimensional four-fold symmetric $SrMoO_4$ dendrite

Cite this: DOI: 10.1039/xoxxoooooox

Hye-Yun Jung and Young-Duk Huh*

Received ooth January 2012,
Accepted ooth January 2012

DOI: 10.1039/xoxxoooooox

www.rsc.org/

A variety of $SrMoO_4$ morphologies were prepared by performing a solvothermal reaction in water–hexane bilayer solutions. The morphology of $SrMoO_4$ crystals evolved from tetragonal bipyramidal to two-dimensional (2-D) four-fold symmetric dendrites as the reaction temperature and the MoO_4^{2-} ion to Sr^{2+} ion reaction concentration ratio were increased. As the reaction temperature increased, the intensity ratio of the (004) to (112) XRD peaks increased dramatically, confirming that the morphology changed from a tetragonal bipyramid to a 2-D four-fold symmetric dendrite. Each of the 2-D four-fold symmetric $SrMoO_4$ dendrites featured four long trunks along the <110> directions and a series of two branches perpendicular to the trunk. A possible crystal growth mechanism for the 2-D four-fold symmetric dendrites was proposed based on the crystallographic evidence.

Introduction

The morphology of a crystalline inorganic oxide may be controlled by tuning the synthetic reaction condition. This approach has been investigated extensively in an effort to understand the relationship between the surface crystal facet reactivity and the physical properties of the crystalline product.[1-7] The crystalline growth of an inorganic oxide depends strongly on the atomic arrangement of the outer facets, which depends on the inorganic oxide morphology. The reactivity and adsorption properties of cubic inorganic oxides with {100} facets differ from the properties of octahedral inorganic oxides with {111} facets or rhombic dodecahedral inorganic oxides with {110} facets.[8-15] Most studies of the synthetically-controlled product morphology have focused on simple closed shapes, such as cubes, octahedra, or rhombic dodecahedra, in which the surfaces are entirely enclosed by six {100}, eight {111}, or twelve {110} facets, respectively.[16-20] These closed shapes, including cubes, octahedra, and rhombic dodecahedra, may be easily prepared by hydrothermal reactions under thermodynamically controlled reactions with the assistance of surfactants that can act as morphological modifiers. Simple open shapes, such as tetrapods, hexapods, and octapods, may be prepared using kinetically controlled reactions under far-from-equilibrium conditions.[21-24] The hierarchical open shapes of inorganic oxides are useful for obtaining more complex catalytic and adsorptive properties from the materials. The crystal growth mechanism and reaction conditions of hierarchical superstructures are more complex than the corresponding properties of simple structures. It is relatively difficult to prepare hierarchical superstructures of inorganic oxides, such as hyper-branches, snowflakes, and dendrites.[25-34] Most studies of hierarchical superstructure morphologies prepared *via* synthetic control have focused on generating the final stable structures rather than on accessing a variety of structures through fine adjustments to the reaction conditions. The crystal growth behaviors and mechanisms must be examined to understand the formation of hierarchical inorganic oxide superstructures.

$SrMoO_4$ is widely used as a Raman converter and host material in light-emitting phosphors.[35,36] A variety of $SrMoO_4$ crystal morphologies, including fishbone-like, octahedral, double taper-like, penniform, and nanorod morphologies, have been obtained using precipitation, hydrothermal reactions, and microemulsion processes.[37-41] Relatively little is known about the evolutionary morphologies of hierarchical $SrMoO_4$ superstructures. This paper reports a method for evolving the morphologies from a tetragonal bipyramid to a two-dimensional (2-D) four-fold symmetric dendrite by adjusting the solvothermal reaction conditions in a water–hexane bilayer system. To the best of our knowledge, this is the first successful preparation of 2-D four-fold symmetric $SrMoO_4$ dendrites. A possible crystal growth mechanism for obtaining 2-D four-fold symmetric dendrites from tetragonal bipyramids is discussed.

Experimental

$Sr(NO_3)_2$ (Aldrich), $Na_2MoO_4{\cdot}2H_2O$ (Aldrich), sodium oleate ($C_{17}H_{33}COONa$, TCI), oleic acid ($C_{17}H_{33}COOH$, Aldrich), and oleylamine ($C_{18}H_{35}NH_2$, TCI) were used without further purification. The 2-D four-fold symmetric $SrMoO_4$ dendrites were obtained from aqueous strontium solutions prepared by adding 2 mmol $Sr(NO_3)_2$, 1.22 g sodium oleate, and 5 mL oleic acid to 10 mL water followed by stirring for 30 min. A 40 mL volume of hexane was then added to each aqueous strontium

solution to form a water–hexane bilayer system. The bilayer solution was vigorously stirred for 1 h to produce an opaque hexane suspension of a strontium oleate complex as a result of a phase transfer reaction. A volume of 0.5 mL oleylamine was added to the bilayer solution with slow stirring over 5 min. A clear transparent suspension of the strontium oleate complex in hexane was then obtained. 30 mL of the transparent strontium oleate complex suspension in hexane was added to 10 mL of a 0.4 M $Na_2MoO_4{\cdot}2H_2O$ aqueous solution to prepare a water–hexane bilayer reaction system. Finally, this bilayer solution was heated to 200°C for 1 h in a 100 mL Teflon-lined autoclave. The rise time period for the reaction temperature was approximately 30 min. The fall time period was reduced to 10 min by immersing the reaction vessel in an ice water bath after each reaction had gone to completion. The $SrMoO_4$ product was washed several times with hexane and ethanol and dried for 24 h at room temperature. The crystal growth mechanism and morphological evolution of $SrMoO_4$ products were investigated as a function of the reaction temperature (120, 130, 160, and 200°C), holding all other conditions constant. At a fixed temperature of 160°C, the concentration of $Na_2MoO_4{\cdot}2H_2O$ was varied to examine the morphological evolution of $SrMoO_4$ products, depending on the concentration ratio of MoO_4^{2-} to Sr^{2+} ions. For comparison, simple hydrothermal reactions were performed without a strontium oleate complex. In a typical synthesis of $SrMoO_4$ crystals using a hydrothermal reaction, 25 mL of an 0.08 M $Sr(NO_3)_2$ aqueous solution was added to 25 mL of an 0.08 M $Na_2MoO_4{\cdot}2H_2O$ aqueous solution and the reaction was stirred for 10 min. The mixed aqueous solution was heated to 120°C (130, 160, or 200°C) for 1 h in a 100 mL Teflon-lined autoclave.

The crystal structures of the $SrMoO_4$ products were characterized using powder X-ray diffraction (XRD, PANalytical, X'Pert-ProMPD). The morphologies of the $SrMoO_4$ products were examined using scanning electron microscopy (SEM, Hitachi S-4300) and transmission electron microscopy (TEM, JEOL JEM-2100F). The presence of capping surfactants on the outer surfaces of the $SrMoO_4$ products was confirmed from the Fourier transform infrared (FT-IR) spectra measured using a Perkin Elmer 100 FT-IR spectrometer.

Results and discussion

Figure 1 shows the scanning electron microscopy (SEM) images of $SrMoO_4$ crystals prepared at various reaction temperatures. At 120°C, rough tetragonal bipyramids with a mean size of 4–5 μm were formed, as shown in Figures 1(a) and 1(b). As the reaction temperature was increased to 130°C, unique three-dimensional (3-D) cross-like shapes were observed, as shown in Figures 1(c) and 1(d). As the reaction temperature was further increased to 160°C, 2-D four-fold symmetric dendrites with one longer trunk and a series of two branches perpendicular to the trunk were obtained, as shown in Figures 1(e) and 1(f). Some T-shaped dendrites, which appeared to be broken parts of a 2-D four-fold symmetric dendrite, were also observed. Perfect 2-D four-fold symmetric dendrites with a mean trunk length of 60–100 μm were obtained at 200 °C, as shown in Figures 1(g) and 1(h). A high-magnification SEM image of an individual 2-D four-fold symmetric dendrite revealed that four long trunks formed a cross-like shape with a series of paired branches arranged perpendicularly to the trunk. The paired branches were arranged parallel to the adjacent branches along the longest axis of the trunk. The branch length was slightly smaller in branches at positions along the dendrite trunk that were further away from the center of the cross. These branches also formed alternating patterns. We confirmed that the morphology of the $SrMoO_4$ crystals evolved from a tetragonal bipyramid through a 3-D cross-like structure to a 2-D four-fold symmetric dendrite as the reaction temperature increased. The trunk length in the four-fold symmetric dendrites also increased with the reaction temperature.

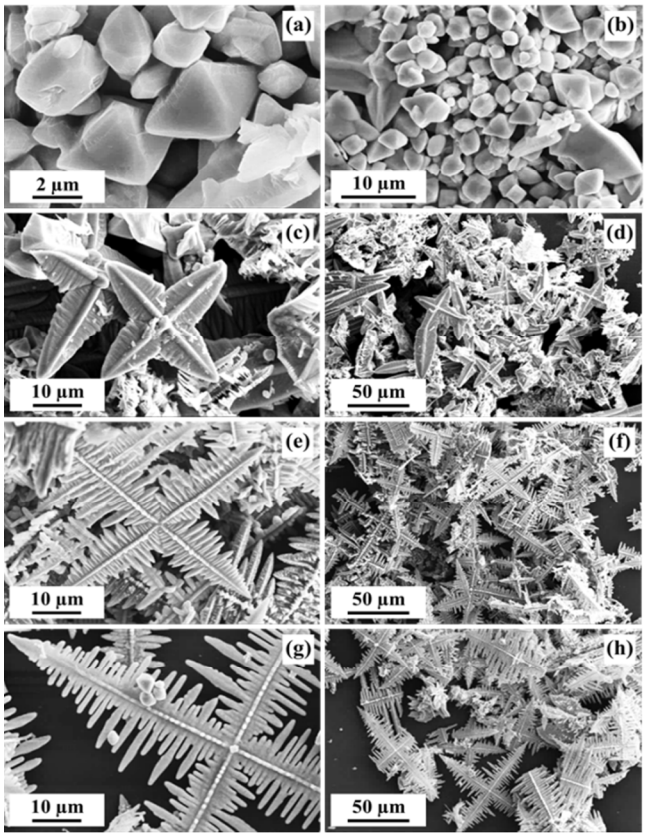

Figure 1. (a, c, e, and g) High-magnification and (b, d, f, and h) low-magnification SEM images of the $SrMoO_4$ products prepared using a solvothermal reaction in a water–hexane bilayer system at various reaction temperatures: (a, b) 120°C, (c, d) 130°C, (e, f) 160°C, and (g, h) 200°C.

Figure 2 shows the X-ray diffraction (XRD) patterns of the $SrMoO_4$ products prepared at various reaction temperatures. All XRD peaks agreed well with the data reported for tetragonal $SrMoO_4$ (JCPDS 08-0482, a = 0.5394 nm, and c = 1.2020 nm). The XRD peak intensity ratios of (004) to (112) were 0.28, 2.06, 2.07, or 2.03 at reaction temperatures of 120, 130, 160, or 200°C, respectively. The XRD intensity ratio of (004) to (112) in the tetragonal $SrMoO_4$

(JCPDS 08-0482) was 0.16. The (004) to (112) ratio increased dramatically at reaction temperatures exceeding 130°C. This result suggested that $SrMoO_4$ products prepared above 130°C presented surfaces with (004) crystal facets, indicating that the 2-D four-fold symmetric dendrites were arranged perpendicular to the crystallographic *c*-axis, as observed in the high-resolution SEM images shown in Figure 1(g).

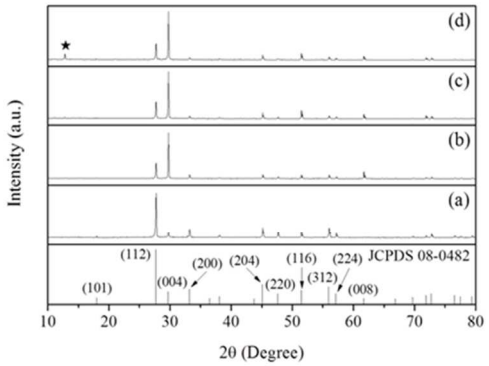

Figure 2. XRD pattern of $SrMoO_4$ products prepared using a solvothermal reaction in a water–hexane bilayer system at various reaction temperatures: (a) 120°C, (b) 130°C, (c) 160°C, and (d) 200°C. The asterisk in (d) indicates unreacted $Na_2MoO_4 \cdot 2H_2O$.

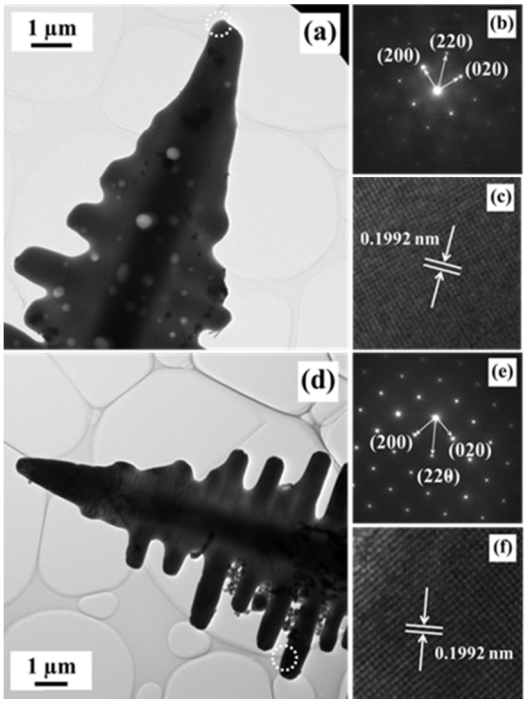

Figure 3. (a) TEM image of an individual $SrMoO_4$ 2-D four-fold symmetric dendrite prepared at 200°C. (b) SAED patterns and (c) HRTEM fringe patterns obtained at the tip of the trunk of a $SrMoO_4$ dendrite. (d) Different TEM image of another part of the2-D four-fold asymmetric dendrites of $SrMoO_4$ productprepared at 200°C. (e) SAED patterns and (f) HRTEM fringe patterns obtained at the tip of a branch of the $SrMoO_4$ dendrite.

Figure 3(a) shows a transmission electron microscopy (TEM) image of an individual 2-D four-fold symmetric $SrMoO_4$ crystal dendrite. Figures 3(b) and 3(c) show selected area electron diffraction (SAED) patterns and high-resolution TEM (HRTEM) fringe patterns measured at the tip of the trunk, respectively. The electron diffraction patterns indicated that the trunk of the 2-D four-fold symmetric $SrMoO_4$ dendrite crystals grew along the four <110> directions. The 0.1992 nm spacing measured in the XRD pattern was nearly equal to the distance (0.1907 nm) between the (220) lattice planes in a tetragonal $SrMoO_4$ crystal. The (220) plane of HRTEM fringe pattern is located perpendicular to the axis of the trunk. Moreover, the (220) SAED patterns are along to the axis of the trunk. Therefore, the trunk of the 2-D four-fold symmetric $SrMoO_4$ dendrite crystals grew along the <110> direction. Each $SrMoO_4$ dendrite, therefore, had a 2-D structure with one trunk along the *ab*-axis.

Unfortunately, the very good SAED images and HRTEM fringe patterns of the trunk and branches of the 2-D four-fold symmetric $SrMoO_4$ dendrite in a single crystal were not observed, simultaneously. Therefore, we presented two different sets of TEM images, SAED images, and HRTEM fringe patterns of the trunk and branches of four-fold symmetric $SrMoO_4$ dendrite crystals, as shown in Figures 4(a, b, c) and 4(d, e, f), respectively. We obtained the different TEM image and its SEAD pattern for the branch of the2-D four-fold asymmetric dendrites of $SrMoO_4$ product simultaneously without any artificial rotation. Figures 3(d), 3(e), and 3(f) show TEM image, the SAED patterns, and the HRTEM fringe pattern measured at the tip of the branch, respectively. Similar electron diffraction patterns of the trunk were observed at the tip of the branch, suggesting that the whole dendrite was a single crystal. The (220) planes were located perpendicular to the branch axis, indicating that branches perpendicular to the trunk were oriented along the other *ab*-axis.

The tetragonal bipyramid of a tetragonal crystal system is one of the most thermodynamically stable closed morphologies. Four-fold symmetric dendrite morphologies are typically formed through kinetically controlled crystal growth processes. The morphological evolution of $SrMoO_4$ crystals from a tetragonal bipyramid to a 2-D four-fold symmetric dendrite suggests that $SrMoO_4$ crystal growth may transition from a thermodynamically controlled reaction to a kinetically controlled reaction as the reaction temperature is increased.

Strontium oleate complexes in hexane play an important role in forming a variety of $SrMoO_4$ crystal morphologies *via* solvothermal reactions in water–hexane bilayer solutions. Because Sr^{2+} ions interact strongly with oleate anions due to the very large strontium oleate complex formation constant, free Sr^{2+} ions are released slowly during a solvothermal reaction. At 120°C, very small amounts of free Sr^{2+} ions are released through the slow decomposition of strontium oleate complexes in hexane. Under these conditions, slow crystal growth can proceed to form thermodynamically stable structures, leading to a tetragonal bipyramid shown in Figure 1(a). Reaction temperatures approaching 200°C favor the fast decomposition of strontium oleate complexes in hexane, and 2-D four-fold symmetric dendrites may be formed under kinetically controlled crystal growth. Dendrites can grow along the four <110> axis directions to form four-trunk dendrites. The second reaction occurs to form branches perpendicular to the trunk. The $SrMoO_4$ crystal morphology changed from a thermodynamically controlled

tetragonal bipyramid to a kinetically controlled 2-D four-fold symmetric dendrite as the reaction temperature increased.

The formation of 2-D four-fold symmetric dendrites through growth along the <110> axis direction was explored by examining the crystal structure of a tetragonal $SrMoO_4$ product. Figure 4(a) shows the scheelite-type lattice structure of $SrMoO_4$, which belongs to the tetragonal space group $I4_1/a$ with $a = b = 0.5394$ nm and $c = 1.2020$ nm. Each Mo site was surrounded by four equivalent O sites arranged in tetragonal symmetry. In the $SrMoO_4$ structure, hard $(MoO_4)^{2-}$ anions were surrounded by Sr^{2+} ions to balance the charges.[42] Figure 4(b) shows a simplified diagram of the $SrMoO_4$ structure with the ten Mo sites located around the central Sr^{2+} ion. The shortest distance between the Mo sites and the central Sr^{2+} ion was 0.3814 nm. The Mo sites were located along the four <110> axis directions. The distance between the Mo sites along the two <001> directions and the central Sr^{2+} ion, however, was 0.6010 nm. The reaction rate for the formation of $SrMoO_4$ along the <110> direction was much faster than the corresponding reaction rate along on the <001> direction. This indicated that crystal growth along the four <l10> directions was preferred at higher reaction temperatures, leading to the formation of a 2-D four-fold symmetric dendrite. Figures 4(c) and 4(d) show atomic arrangements {112} and {110} facets, respectively. Unit cell length of *c*-axis is almost twice longer than that of *a*-axis. Figure 4(e) shows a schematic diagram for the formation of elongated tetragonal and octahedron-like tetragonal morphologies covered by {111} facets and {112} facets.

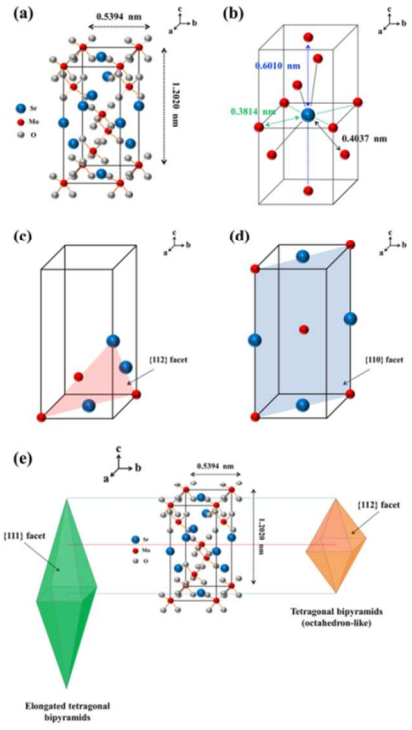

Figure 4. The scheelite-type $SrMoO_4$ crystal structure in the tetragonal space group $I4_1/a$, with $a = b = 0.5394$ nm and $c = 1.2020$ nm. (b) Simplified diagram of the $SrMoO_4$ structure with ten Mo sites around the central Sr^{2+} ion. The crystal structures of (c) {112} and (d) {110} facets. (e) Schematic diagram for the formation of elongated tetragonal and octahedron-like tetragonal morphologies covered by {111} facets and {112} facets.

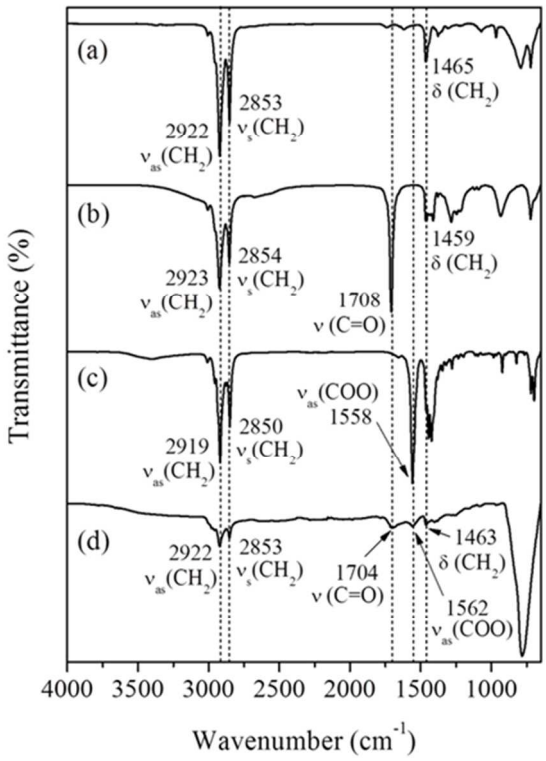

Figure 5. FT-IR spectra of (a) oleylamine, (b) oleic acid, (c) sodium oleate, and (d) the $SrMoO_4$ product prepared at 200°C.

FT-IR spectra provide information about the capped organic molecules present on the surfaces of $SrMoO_4$ products. Figure 5 shows the FT-IR spectra of the oleylamine, oleic acid, sodium oleate, and $SrMoO_4$ products. The FT-IR spectrum of $SrMoO_4$ revealed strong peaks at 2922 cm^{-1}, 2853 cm^{-1}, and 1463 cm^{-1} that were assigned, respectively, to the asymmetric stretching, symmetric stretching, and symmetric bending vibrations of the methylene group (-CH_2-). A 1708 cm^{-1} carbonyl group stretching mode characteristic of oleic acid and a 1558 cm^{-1} carboxylate group stretching mode characteristic of sodium oleate were observed in the FT-IR spectrum of the $SrMoO_4$ product.[43] These results indicated that the $SrMoO_4$ products were capped mainly by both sodium oleate and oleic acid. The broad strong absorption band at 760 cm^{-1} was related to the stretching mode of the MoO_4 tetrahedron in the $SrMoO_4$ product.[44] Figure 6 shows SEM images of $SrMoO_4$ products prepared at 160°C *via* a water–hexane bilayer solvothermal reaction, under various concentrations of $Na_2MoO_4 \cdot 2H_2O$ at a fixed concentration of strontium nitrate. A ratio of $[MoO_4^{2-}]/[Sr^{2+}] = 0.25$ yielded tetragonal bipyramids with a mean size of 4–5 μm, as shown in Figures 6(a) and 6(b). A ratio of $[MoO_4^{2-}]/[Sr^{2+}] = 0.50$ yielded both 4–5 μm tetragonal bipyramids and elongated twinned 6-7μm taper, as shown in Figures 6(c) and 6(d). The arms of the elongated twinned tapers were slightly notched. A $[MoO_4^{2-}]/[Sr^{2+}]$ ratio of 1.0 yielded an elongated twinned taper, as shown in Figures 6(e) and 6(f). The length of the four-fold symmetric elongated twinned taper increased to 20–40 μm. The elongated twinned taper formed a deep concave shape with large open spaces. Four small arms were

observed at the center. A $[MoO_4^{2-}]/[Sr^{2+}]$ ratio of 2.0 yielded distinct 2-D four-fold symmetric dendrites, as shown in Figures 6(g) and 6(h). The XRD peak intensity ratios of (004) to (112) were 0.31, 0.27, 0.38, and 2.07 for $[MoO_4^{2-}]/[Sr^{2+}]$ ratios of 0.25, 0.50, 1.0, and 2.0, respectively. A $[MoO_4^{2-}]/[Sr^{2+}]$ ratio of 2.0 yielded a dramatically higher intensity ratio of (004) to (112). These results indicated that plate-like 2-D dendrites were only observed at $[MoO_4^{2-}]/[Sr^{2+}]$ = 2.0. The 2-D four-fold symmetric dendrites formed at higher concentrations of $Na_2MoO_4{\cdot}2H_2O$ under the kinetically controlled reaction conditions.

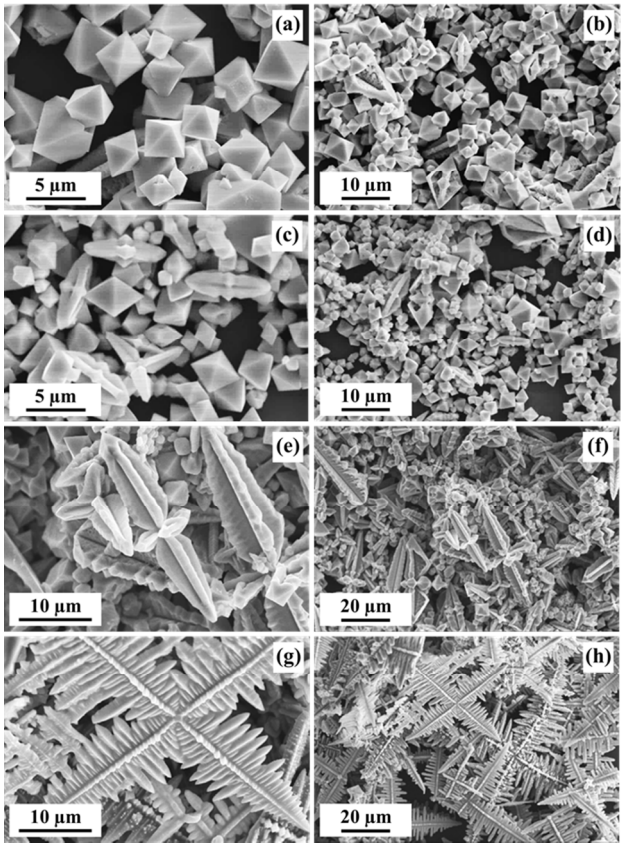

Figure 6. (a, c, e, and g) High-magnification and (b, d, f, and h) low-magnification SEM images of the $SrMoO_4$ products prepared using a solvothermal reaction in a water–hexane bilayer system with various $[MoO_4^{2-}]/[Sr^{2+}]$ reaction concentration ratios: (a, b) 0.25, (c, d) 0.50, (e, f) 1.0, and (g, h) 2.0.

To examine the effect of the water-hexane bilayer reaction system, $SrMoO_4$ crystals were also prepared by performing hydrothermal reactions in the absence of the strontium oleate complex for comparison. Self-assembled peanut-like $SrMoO_4$ crystals were obtained, regardless of the reaction temperature, as shown in Figure 7. The nanoparticles formed through a direct rapid reaction between free Sr^{2+} ions and MoO_4^{2-} ions in the hydrothermal reaction. The nanoparticles easily self-assembled to form $SrMoO_4$ crystals resembling peanuts with round faces at the ends. Figure 8 shows XRD pattern of $SrMoO_4$ products prepared using a hydrothermal reaction in the absence of a strontium oleate complex. All XRD peaks agreed well with the reported for tetragonal $SrMoO_4$ (JCPDS 08-0482). However, the peak intensity of (004) is much weaker than that of the 2-D four-fold symmetric dendrite, as shown in Figure 2(d). It indicated that 2-D four-fold symmetric dendrites covered by {004} facets were not prepared in a hydrothermal reaction.

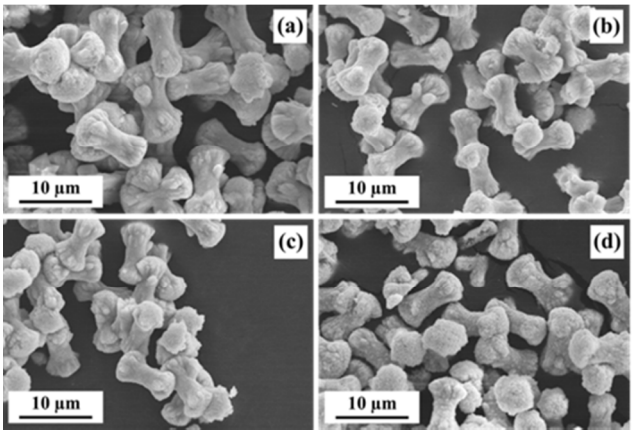

Figure 7. SEM images of the $SrMoO_4$ products prepared using a hydrothermal reaction in the absence of a strontium oleate complex at various reaction temperatures: (a) 120°C, (b) 130°C, (c) 160°C, and (d) 200°C.

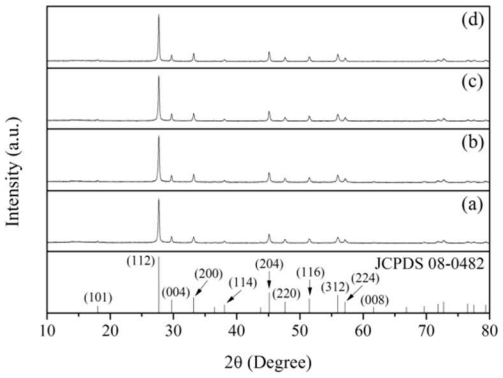

Figure 8. XRD pattern of $SrMoO_4$ products prepared using a hydrothermal reaction in the absence of a strontium oleate complex at various reaction temperatures: (a) 120°C, (b) 130°C, (c) 160°C, and (d) 200°C.

$SrMoO_4$ crystals were also prepared by performing hydrothermal reactions in the presence of the strontium oleate complex in aqueous solution without adding of hexane. In this case, we used the same reaction condition for the solvothermal water-hexane bilayer system, except adding the hexane and phase transfer for the formation of strontium oleate complex in hexane. Therefore, strontium oleate complex was form in the aqueous solution instead of in the hexane of the water-hexane bilayer system. Figure 8 shows SEM images of the micron-sized ellipsoidal $SrMoO_4$ morphology aggregated from smaller particles with a few hundred nanometer length. Therefore, direct and rapid reaction for the formation of nano-sized $SrMoO_4$ particles is occurred even in the presence of the strontium oleate

complex in the hydrothermal reaction. The similar aggregated micron-sized crystal formation behaviour was observed in hydrothermal reaction in the absence of the strontium oleate complex, as shown in Figure 7. In the hydrothermal reaction system, the interaction of between Sr^{2+} ions and MoO_4^{2-} ions is stronger than that of between Sr^{2+} ions and oleate ions. It indicates that the strontium oleate complex in aqueous solution does not play important role in formation of any branched structures, such as 2-D four-fold symmetric dendrites. Therefore, we found that the water-hexane bilayer reaction system was critical for the formation of 2-D four-fold symmetric dendrites.

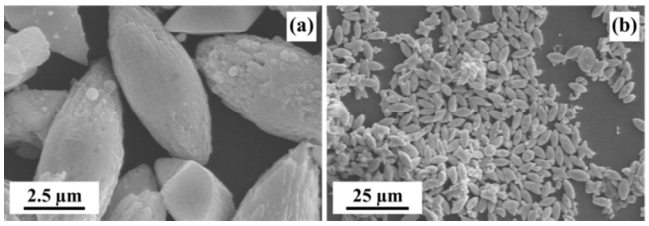

Figure 9. (a) High-magnification and (b) low-magnification SEM images of the $SrMoO_4$ products prepared using a hydrothermal reaction in the presence of a strontium oleate complex in aqueous solution without adding of hexane at 200°C.

Conclusions

A variety of $SrMoO_4$ morphologies were prepared by adjusting the reaction temperature and reactant $Na_2MoO_4{\cdot}2H_2O$ concentration in a hexane–water bilayer solvothermal reaction system. As the reaction temperature was increased, the morphology evolved from a tetragonal bipyramid to a 3-D cross-like dendrite, and finally to a 2-D four-fold symmetric dendrite. Similarly, the morphology evolved from a tetragonal bipyramid to a 2-D four-fold symmetric dendrite as the reactant $[MoO_4^{2-}]/[Sr^{2+}]$ ratio increased. These results indicated that a tetragonal bipyramid formed under thermodynamically controlled reaction conditions at lower reaction temperatures and smaller $[MoO_4^{2-}]/[Sr^{2+}]$ ratios. By contrast, a 2-D four-fold symmetric dendrite formed under the kinetically controlled reaction conditions at higher reaction temperatures and larger $[MoO_4^{2-}]/[Sr^{2+}]$ ratios. Crystal growth under kinetic control proceeded preferentially along the <110> direction, leading to the formation of a 2-D four-fold symmetric dendrite.

Acknowledgements

This research was supported by the Basic Science Research Program through the National Research Foundation of Korea, funded by the Ministry of Education (NRF-2010-0007492). We would like to thank the Korea Basic Science Institute at the Gangneung Center for support in collecting the TEM images.

Notes and references

Department of Chemistry, Dankook University, Gyeonggi-Do 448-701, Korea.

1. C. Burda, X. Chen, R. Narayanan and M. A.El-Sayed, *Chem. Rev.* 2005, **105**, 1025.
2. M. H. Huang, S. Rej and S. -C. Hsu, *Chem. Commun.* 2014, **50**, 1634.
3. X. Zhao, Z. Bao, C. Sun and D. Xue, *J. Cryst. Growth* 2009, **311**, 711.
4. M. H. Huang and C. -Y. Chiu, *J. Mater. Chem. A* 2013, **1**, 8081.
5. X. Lan, J. Zhang, H. Gao and T. Wang, *CrystEngComm* 2011, **13**, 633
6. S. Sun, C. Kong, S. Yang, L. Wang, X. Song, B. Ding and Z. Yang, *CrystEngComm* 2011, **13**, 2217.
7. M. -J. Kim, Y. -S. Cho, S. -H. Park and Y. -D. Huh, *Cryst. Growth Des.* 2012, **12**, 4180.
8. Q. Hua, T. Cao, X. K. Gu, J. Lu, Z. Jiang, X. Pan, L. Luo, W. X. Li and W. Huang, *Angew. Chem. Int. Ed.* 2014, **53**, 4856.
9. H. Xu, W. Wang and W. Zhu, *J. Phys. Chem. B* 2006, **110**, 13829.
10. G. Wang, X. Ma, B. Huang, H. Cheng, Z. Wang, J. Zhan, X. Qin, X. Zhang and Y. Dai, *J. Mater. Chem.* 2012, **22**, 21189.
11. L. Zhang, J. Shi, M. Liu, D. Jing and L. Guo, *Chem. Commun.* 2014, **50**, 192.
12. C. H. Kuo and M. H. Huang, *Nano Today* 2010, **5**, 106.
13. Y. -J. Lee, S. Kim, S. -H. Park, H. Park and Y. -D. Huh, *Mater. Lett.* 2011, **65**, 818.
14. D. -F. Zhang, H. Zhang, L. Guo, K. Zheng, X. D. Han and Z. Zhang, *J. Mater. Chem.* 2009, **19**, 5220.
15. Y. Zhang, B. Deng, T. Zhang, D. Gao and A. -W. Xu, *J. Phys. Chem. C* 2010, **114**, 5073.
16. J. -Y. Ho and M. H. Huang, *J. Phys. Chem. C* 2009, **113**, 14159.
17. C. -H. Kuo and M. H. Huang, *J. Phys. Chem. C* 2008, **112**, 18355.
18. C. -H. Kuo, C. -H. Chen and M. H. Huang, *Adv. Funct. Mater.* 2007, **17**, 3773.
19. X. Wang, H. -F. Wu, Q. Kuang, R. -B. Huang, Z. -X. Xie and L. -S. Zheng, *Langmuir* 2010, **26**, 2774.
20. Q. Hua, D. Shang, W. Zhang, K. Chen, S. Chang, Y. Ma, Z. Jiang, J. Yang and W. Huang, *Langmuir* 2011, **27**, 665.
21. L. Wang, B. Liu, S. Ran, H. Huang, X. Wang, B. Liang, D. Chen and G. Shen, *J. Mater. Chem.* 2012, **22**, 23541.
22. Z. -Z. Chen, E. -W. Shi, Y. -Q. Zheng, W. -J. Li, B. Xiao and J. -Y. Zhuang, *J. Cryst. Growth* 2003, **249**, 294.
23. Z. -H. Liang and Y. -J. Zhu, *Mater. Lett.* 2005, **59**, 2423.
24. Y. -J. Lee and Y. -D. Huh, *Mater. Res. Bull.* 2011, **46**, 1892.
25. B. Liu, S. –H. Yu, L. Li, Q. Zhang, F. Zhang and K. Jiang, *Angew. Chem. Int. Ed.* 2004, **43**, 4745.
26. M. Cao, T. Liu, S. Gao, G. Sun, X. Wu, C. Hu and Z. L. Wang, *Angew. Chem. Int. Ed.* 2005, **44**, 4197.
27. G. Sun, B. Dong, M. Cao, B. Wei and C. Hu, *Chem. Mater.* 2011, **23**, 1587.
28. S. Bharathi, D. Nataraj, M. Seetha, D. Mangalaraj, N. Ponpandian, Y. Masuda, K. Senthil and K. Yong, *CrystEngComm* 2010, **12**, 373.
29. Y. Jiao, Y. Liu, F. Qu and X. Wu, *CrystEngComm* 2014, **16**, 575.
30. M. Hu, J. -S. Jiang and X. Li, *Cryst.Growth Des.* 2009, **9**, 820.
31. Y. Cheng, Y. Wang, D. Chen and F. Bao, *J. Phys. Chem. B* 2005, **109**, 794.
32. Q. Gong, X. Qian, H. Cao, W. Du, X. Ma and M. Mo, *J. Phys. Chem. B* 2006, **110**, 19295.
33. X. Zhang, Y. Xie, F. Xu and X. Tian, *J. Colloid Interface Sci.* 2004, **274**, 118.
34. Y. -S. Cho and Y. -D. Huh, *Mater. Lett.* 2011, **65,** 3618.

35. T. T. Basiev, A. A. Sobol, Y. K. Voronko and P. G. Zverev, *Opt. Mater.*2000, **15**, 205.
36. Y. -F. Liu, S. -H. Dai, Y. -N. Lu and H. –H. Min, *Powder Technol.* 2012, **221**, 412.
37. Q. Gong, X. Qian, X. Ma and Z. Zhu, *Cryst. Growth Des.* 2006, **6**, 1821.
38. W. Jiang, W. Zhu, C. Peng, F. Yang, S. Xuan and X. Gong, *Cryst. Res. Technol.* 2012, **9**, 997.
39. G. Xing, Y. Li, Y. Li, Z. Wu, P. Sun, Y. Wang, C. Zhao and G. Wu, *Mater. Chem. Phys.* 2011, **127**, 465.
40. S. Lei, X. Peng, X. Li, Z. Liang, Y. Yang, B. Cheng, Y. Xiao and L. Zhou, *Mater. Res. Bull.* 2011, **46**, 601.
41. E. -J. Choi and Y. -D. Huh, *Bull. Kor. Chem. Soc.* 2010, **31**, 196.
42. D. Errandonea, R. S. Kumar, X. Ma and C. Tu, *J. Solid State Chem.* 2008, **181**, 355.
43. W. Bu, Z. Chen, F. Chen and J. Shi, *J. Phys. Chem. C* 2009, **113**, 12176.
44. T. Thongtem, A. Phuruangrat and S. Thongtem, *Mater. Lett.* 2008, **62**, 454.

Graphical abstract

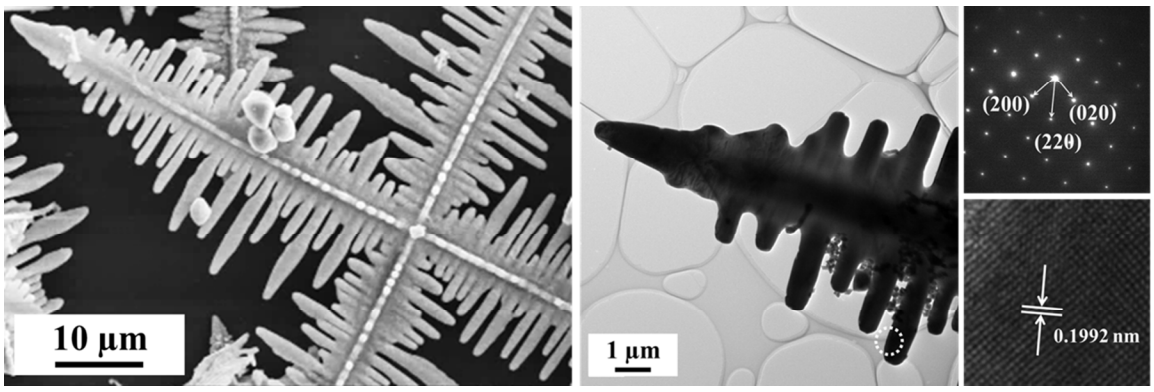

Highlight : The morphology evolution of $SrMoO_4$ microcrystals were obtained from a tetragonal bipyramid to a 3-D cross-like dendrite, and finally to a 2-D four-fold symmetric dendrite.